Electric field modeling in heavily irradiated silicon detectors based on Edge-TCT measurements[*]

Gregor Kramberger[†][a], **V. Cindro**[a], **I. Mandić**[a], **M. Mikuž**[a,b], **M. Milovanović**[a], **M. Zavrtanik**[a] [‡]

[a] *Jozef Stefan Institute*

[b] *University of Ljubljana, Faculty of Mathematics and Physics, Department of Physics*

E-mail: Gregor.Kramberger@ijs.si

Velocity profiles in heavily irradiated silicon micro-strips detector were investigated by Edge-TCT. The parameters of a simple electric field model assuming two space charge regions at each side of the detector and neutral bulk in-between were extracted from the measurements.

---

1. Introduction

Recent advances in position sensitive silicon detectors have extended their usability to most hostile radiation environments envisaged at an upgraded Large Hadron Collider (HL-LHC). There the most exposed tracking and vertexing detectors will be exposed to fluences of fast hadrons in excess of $1.6 \cdot 10^{16}$ cm^{-2} [1]. The displaced silicon atoms which arise from the collisions with impinging particles lead to emergence of energy levels in the band-gap, which lead to deterioration of detector performance. The radiation damage manifests mainly in increase of: generation current, space charge and trapping of the drifting charge [2].

If a decade ago the use of silicon detectors beyond 10^{15} fast hadrons/cm^2 was seen as a major challenge [3] it seems now that the combination of: readout at segmented n$^+$ electrodes, high voltage operation, carefully planned annealing scenario and proper electrode design leads to efficient operation of detectors over the whole fluence range at HL-LHC [4, 5]. The underlying physics reason for that is the onset of impact ionization [6, 7], which causes charge multiplication and thus improved charge collection with respect to the one expected from extrapolation of measurements at lower fluences.

In order to predict and understand the operation the knowledge of electric field profile is essential. There were many attempts to calculate electric field in an irradiated detector from the energy levels measured with Deep Level Transient Spectroscopy or Thermally Stimulated Current techniques [8, 9], however none of them were able to reproduce the charge collection measurements with proper trap parameters.

Transient current technique (TCT) is a most widely used tool for investigation of the electric field profile in semiconductor detectors [10]. The current induced after generation of free carriers by light pulse is monitored by a fast current amplifier. The shape of the current pulse is proportional to the velocity, hence the electric field profile can be extracted from time evolution of the current pulse. At fluences in the HL-LHC range the trapping distance becomes so short [11, 12] that it is impossible to probe the electric field in the detector bulk from the pulse shape. Electric field at very high fluences can be probed by using TCT in a novel way where the edge of the detector is illuminated with focused IR laser beam - so called Edge-TCT [13]. This technique was used also in this work for establishing the evolution of the electric field in a float zone n-on-p detector at different fluences.

2. Experimental technique and samples

The measurements were performed on a *p*-type micro-strip detector processed by HPK[1] on float zone silicon. The initial resistivity of silicon was around 5 kΩ cm, resulting in a full depletion voltage of $V_{fd} \approx 180$ V for a 300 μm thick detector. The miniature detector had 1 cm long AC coupled n$^+$ strips with a pitch of 100 μm and implant width of 20 μm. It was irradiated in steps with neutrons in the TRIGA nuclear reactor of the Jožef Stefan Institute in Ljubljana [14, 15] up to the equivalent fluence of 10^{16} cm^{-2} (step of $1, 1, 3, 5 \cdot 10^{15}$ cm^2). Between irradiation steps the detector was annealed in steps (10, 10, 20, 40 min) up to accumulated time of 80 min at 60°C - so called CERN scenario measurement. During each annealing step Edge-TCT measurements were

---

[1]Hamamatsu Photonics, Japan

performed at $T = -20°C$. A Peltier element was used for heating and cooling, thus allowing the detector to remain mounted in the setup also during annealing.

The basic principle of the Edge-TCT technique is shown in Fig. 1. The narrow laser beam of infrared light ($\lambda = 1064$ nm, ≈ 40 ps pulses, 200 Hz repetition rate) illuminates a carefully polished edge of the detector. The electron-hole pairs are created almost uniformly along the beam in a similar way as for the minimum ionizing particles. The beam position and by that the depth at which the carriers are generated can be controlled by moving stages with sub-micron precision. In the electric field the carriers start to drift and induce signal in the current amplifier (MITEQ AM-1309, 10 kHz-1 GHz) connected to one of the strips. The average of 400 pulses is taken by a 1.5 GHz oscilloscope at each point. The detailed description of the setup and the measurement technique can be found in Ref. [13].
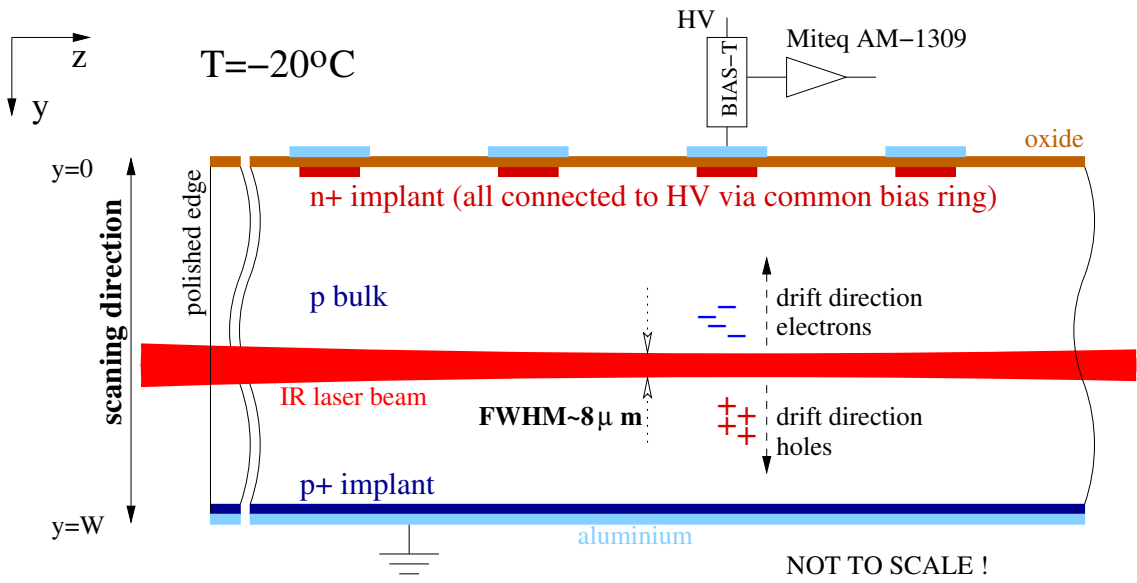

Figure 1: Schematic view of the Edge-TCT technique.

3. Velocity profiles

The induced current I at the time t after generation of electron-hole pairs at depth y in the detector is given by [13]

$$I(y,t) = I_e(y,t) + I_h(y,t) \approx e_0 A N_{e-h} \frac{1}{W} \left[v_e(y,t) e^{-t/\tau_{eff,e}} + v_h(y,t) e^{-t/\tau_{eff,h}} \right] \quad , \qquad (3.1)$$

where y denotes the beam position, e_0 elementary charge, A amplifier amplification, N_{e-h} number of generated electron hole pairs and $v_{e,h}$ the drift velocities averaged over the strip width at given y (see Fig. 1). Note that the weighting field term is effectively $1/W$, where W denotes the detector thickness. This is a consequence of uniform generation of charge underneath the strips [13]. The current amplitude immediately after non-equilibrium carrier generation ($\exp(-t/\tau_{eff,e,h}) \approx 1$) can

therefore be expressed as

$$I(y, t \sim 0) \approx e_0 A N_{e,h} \frac{v_e(y) + v_h(y)}{W} \qquad . \qquad (3.2)$$

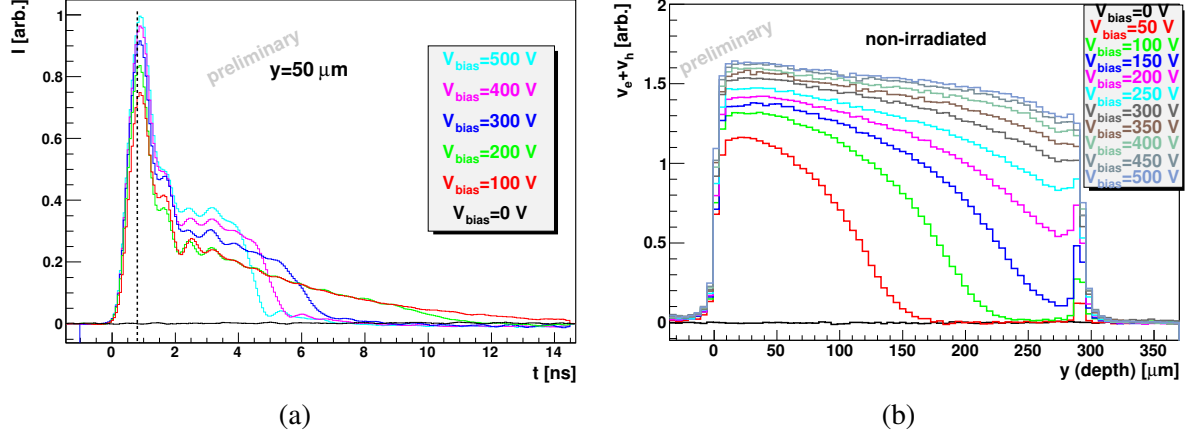Hence the initial rise of the current is proportional to the sum of drift velocities. An example

Figure 2: (a) Induced current pulses in a non-irradiated detector after generation of free carriers at $y = 50$ μm. The initial rise is due to drift of electrons and the long tail due holes. (b) Velocity profiles at different bias voltages.

of induced current pulses at $y = 50$ μm for different bias voltages in an non-irradiated detector is given in Fig. 2a. The value of induced current pulse at ~ 600 ps was taken as the measure of the sum of drift velocities. A scan across the depth was made to produce the velocity profile in the detector. For a non-irradiated detector (Fig. 2b.) it can be clearly seen that the velocity of charges injected in non-depleted bulk vanishes. The difference in doping at the $p^+ - p$ contact results in appearance of electric field even at voltages below $V_{fd} \sim 180$ V. At $V > V_{fd}$ the velocity starts to saturate and there is little difference between profiles at 300 V and 500 V. The velocity profiles of irradiated detector to different fluences is shown if Fig. 3. At the strip side velocity is almost saturated at high bias voltages, except after the last fluence step 10^{16} cm^{-2} where non-negligible rise in pulse height at 600 ps at highest voltages can be attributed to charge multiplication. Apart from the high field region at the strips the drift velocity increases also at the back. Such a profile is known as "double peak electric field profile" [10], but it is for the first time that it is observed at HL-LHC fluences. One should however note that velocity saturates with electric field, therefore the second peak corresponds to significantly smaller electric field (see next sections). In principle it should be straightforward to extract the electric field profile from velocity profile by using $v_e + v_h = \left[\mu_e(E) + \mu_h(E) \right] E$. However at high electric fields the signal becomes insensitive to changes in electric field due to drift velocity saturation. In addition the measured drift velocity profile is an average over the strip. Any lateral dependence of the field which inevitably occurs close to the strips prevents a straightforward extraction of the field. However, a similar shape of the velocity profiles allows for modeling of the field with small number of free parameters.

4. Field modeling

Non-monotonic velocity profiles shown in Figs. 3 can only occur if the space charge changes
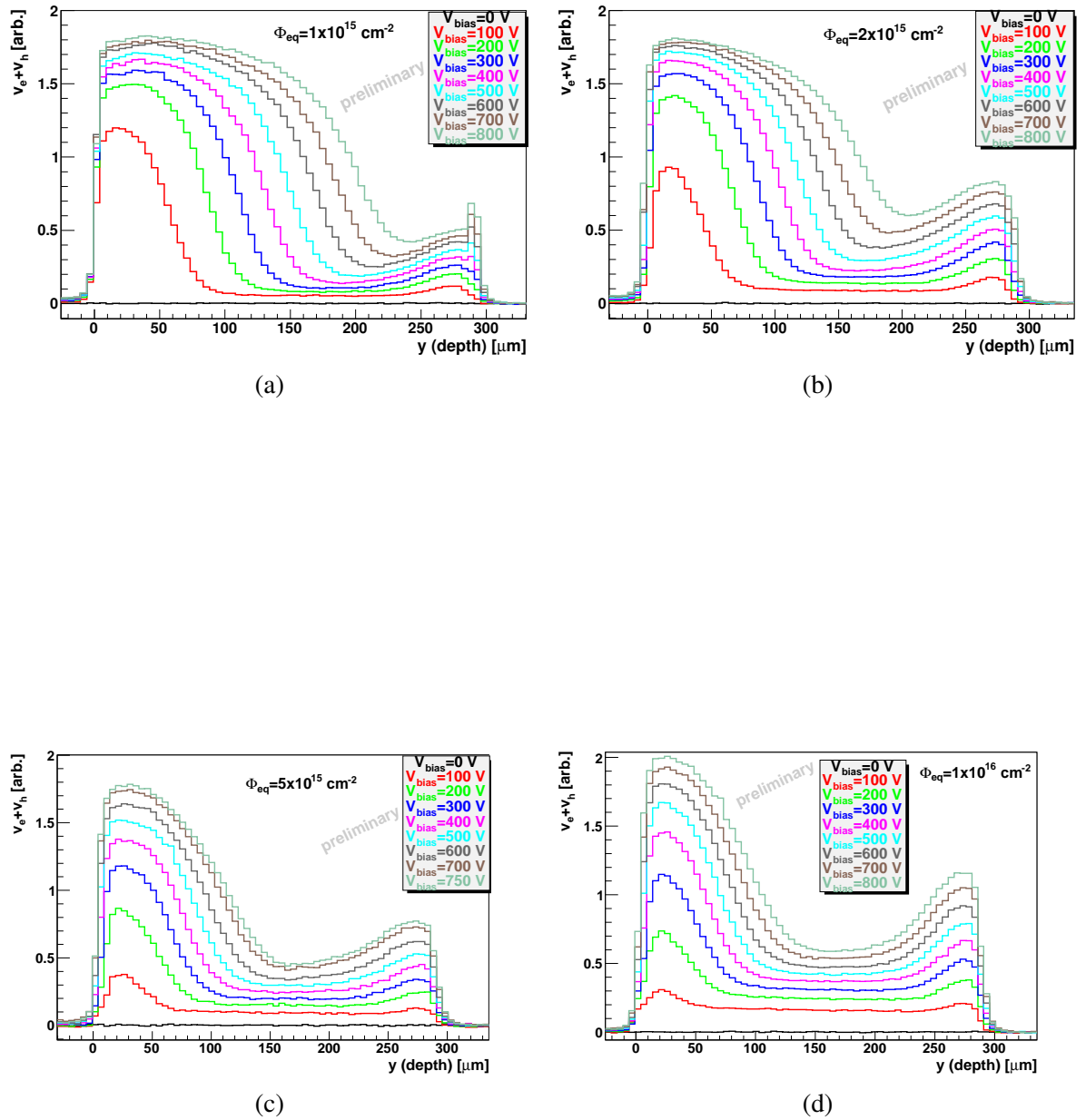
Figure 3: Velocity profiles at different bias voltages for irradiated detector at different fluence steps: (a) $1 \cdot 10^{15}$ cm^{-2}, (b) $2 \cdot 10^{15}$ cm^{-2}, (c) $5 \cdot 10^{15}$ cm^{-2} and (d) $1 \cdot 10^{16}$ cm^{-2}. The profiles shown are after 80 min annealing at each irradiation fraction.

sign inside the detector. A schematic view of the model can be seen in Fig. 4a. The physical reason for such a shape is related to different occupation probability of the traps in presence of enhanced free carrier concentration, electrons and holes, at both ends of the detector [16, 17, 18]. For simplicity reasons the N_{eff} is assumed to be constant in both space charge regions. Such a space charge leads to linear electric field at both ends and constant field in the so called neutral bulk. Although abrupt change is physically unrealistic the model may still serve the purpose of adequate description of measured profiles, hence it was used in the rest of the paper. Moreover,

the change of both regions with voltage, as it will be shown, allows for a conclusion that constant N_{eff} is a good approximation, particularly at lower fluences. In general, one can look at the model parameters, borders of both regions y_{act}, y_{back}, ratio of drift and saturation velocity in the bulk and at the back v_{bulk}/v_{sat}, v_{back}/v_{sat} as constraints that have to be fulfilled for any shape of the $N_{eff}(y)$. An example of determination of parameters is shown in Fig. 4b. A fit of a linear function is made
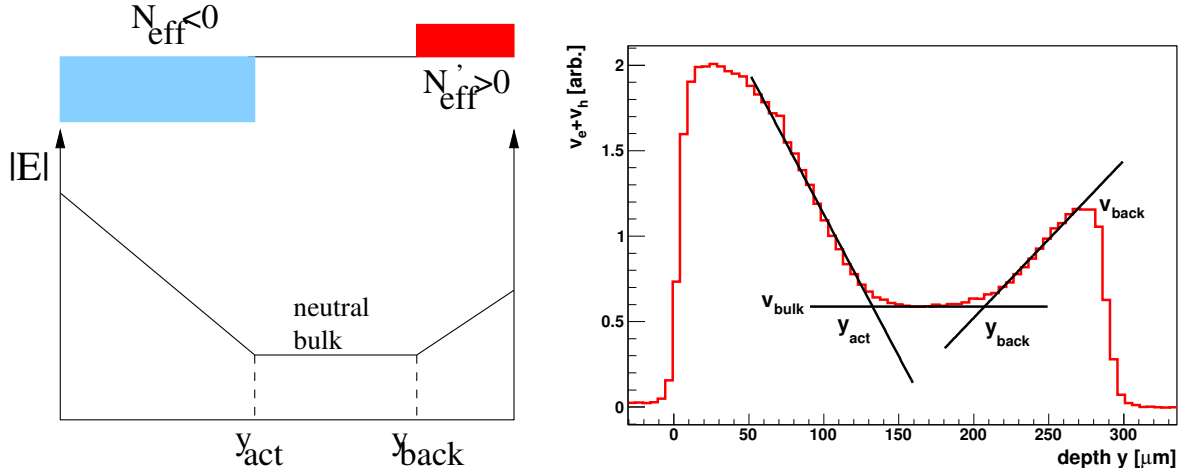

Figure 4: (a) The effective space charge and electric field model used in the work. (b) An example of determination of important model parameters from the measured velocity profile after receiving $1 \cdot 10^{16}$ cm^{-2}, annealed for 80 min at 60°C and biased to 800 V.

on both sides of the space charge regions. Their intersection with constant velocity in neutral bulk determines the y_{act} and y_{back} as well as v_{bulk}/v_{sat}. A value of the linear fit at the back side of the detector gives v_{back}/v_{sat}.

4.1 Active region - junction side

The dependence of the junction region y_{act} on voltage is shown for all fluences after 80 min annealing in Fig. 5a. If constant N_{eff} is assumed and voltage drop in neutral bulk and at back side of detector is neglected than y_{act} should scale as

$$y_{act} = \sqrt{\frac{2\,\varepsilon_{Si}V_{bias}}{e_0 N_{eff}}} \quad . \tag{4.1}$$

where e_0 is elementary charge and ε_{Si} absolute permittivity of Silicon. The fit of the Eq. 4.1 with N_{eff} as free parameter to the data reveals that the agreement is good for lower fluences, while at higher fluences y_{act} is somewhat larger than predicted at low voltages. The fact that y_{act} follows the Eq. 4.1 points to the only weak dependence of $N_{eff}(y)$.

Fig. 5b shows y_{act} at different annealing times. The evolution follows the expected behavior in accordance with Hamburg model (see Fig. 5b)[2]. Initial decrease of active acceptors results in increase of y_{act}. After around 80 min at 60°C the short term annealing is completed. Increase of effective acceptors during the long term annealing occurs on the much longer time scale than that in our measurements and was neglected. This allows for determination of introduction rates of
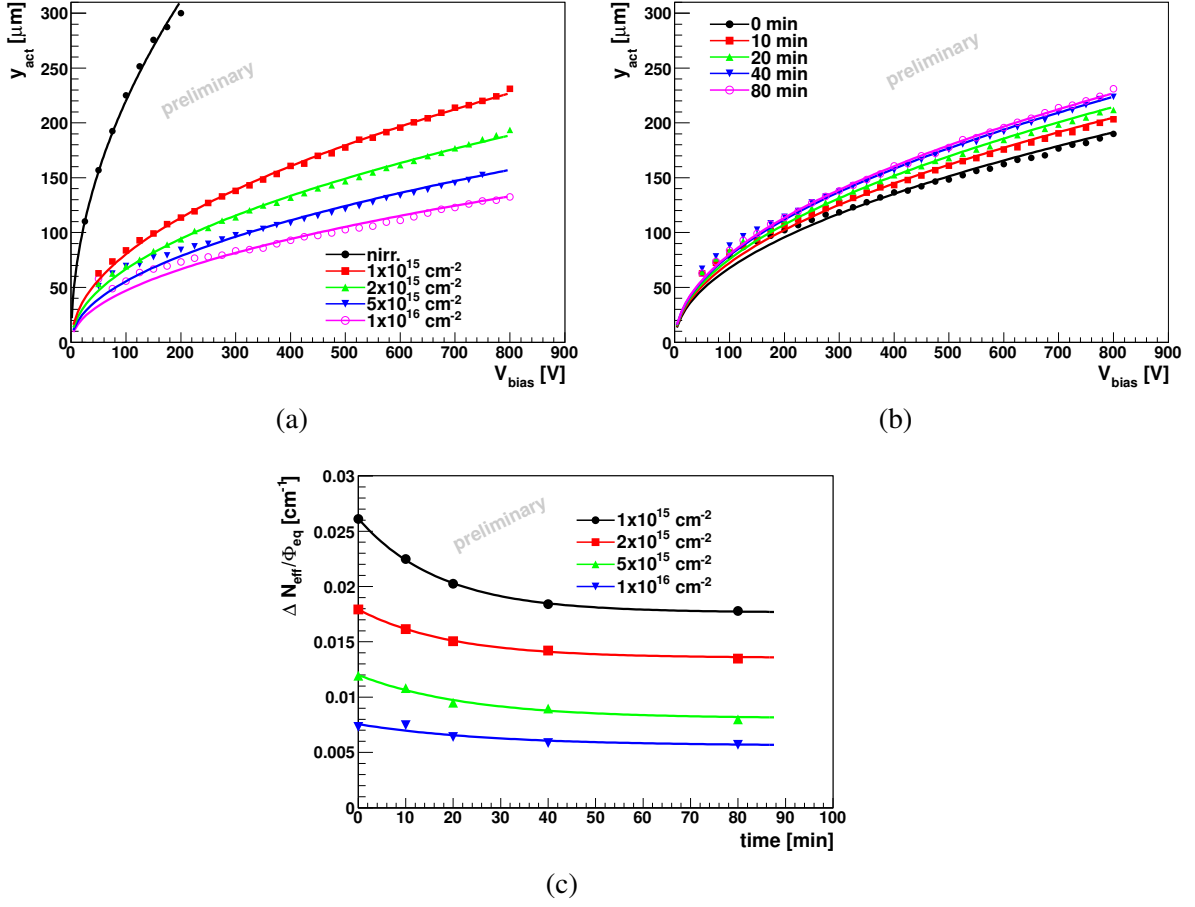
6

(a)

(b)

(c)

Figure 5: (a) Dependence of y_{act} on voltage for different fluences (annealed for 80 min) (b) Dependence of y_{act} on annealing time for the irradiation fluence of $1 \cdot 10^{15}$ cm^{-2}. The fits of the Eq. 4.1 to the data is shown by solid lines. (c) $\Delta N_{eff}/\Phi_{eq}$ vs. annealing time for all fluence steps.

short term and stable damage

$$\frac{\Delta N_{eff}}{\Phi_{eq}} = \frac{N_{eff,0} - N_{eff}}{\Phi_{eq}} \approx g_c + g_{ba} \exp(-t/\tau_{ba}) \quad , \tag{4.2}$$

where g_c denotes the introduction rates of defects stable in time, g_{ba} defects that anneal out with time constant τ_{ba} and $N_{eff,0}$ initial concentration of acceptors. The results are shown in Fig. 5c together with fit of Eq. 4.2 to the data. The parameters determined from the fit g_c, g_{ba}, τ_{ba} are gathered in the Table 1. Up tp $2 \cdot 10^{15}$ cm^{-2} the agreement with low fluence data obtained from C-V is satisfactory. This in turn means that voltage drop in the bulk and at the back contact is small compared to the drop at the junction.

At larger fluences the effective space charge concentration compatible with measured y_{act} is significantly smaller than extrapolated from low fluence measurements. A significantly larger voltage drop at higher fluences in "neutral bulk" and at the back contact, if accounted for, would reduce this effective space charge even further. It is evident that at larger fluences not only that there is significant electric field at the back of the detector and in the bulk, but also the main junction penetrates deeper in the detector bulk than predicted.

Table 1: The parameters obtained from the fit of Eq. 4.2 to the data shown in Fig. 5c. The parameter g_{ba} was calculated from the fit value for each irradiation fractions separately assuming no annealing effects of the previous irradiation fraction. The reference values are $g_c = 0.019$ cm^{-1}, $g_{ba} \approx 0.014 - 0.018$ cm^{-1}, $\tau_{ba} = 21$ min [2] and $g_c = 0.017$ cm^{-1} [19].

Fluence	g_c [cm^{-1}]	g_{ba} [cm^{-1}]	τ_{ba} [min]
$\Phi_{eq} = 10^{15}$ cm^{-2}	0.0176	0.0085	17.2
$\Phi_{eq} = 2 \cdot 10^{15}$ cm^{-2}	0.0135	0.0088	20.5
$\Phi_{eq} = 5 \cdot 10^{15}$ cm^{-2}	0.0078	0.0069	26.25
$\Phi_{eq} = 10^{16}$ cm^{-2}	0.0055	0.0103	31.44

The annealing parameters listed in Table 1 are in agreement with RD48 data at lower fluences. At larger fluences one should bare in mind that the detector was irradiated in several steps and only the part of the damage received in the last fraction undergoes short term annealing. No annealing effects, which may have occured during the irradiation, were taken into account.

4.2 Back electrode

The thickness of the space charge region at the back of the detector doesn't show significant dependence on fluence as can be seen in Fig. 6a. Once the y_{act} approaches the back side of the detector at higher voltages, y_{back} starts to increase again i.e. the back region shrinks, which can be seen for the detector after $\Phi_{eq} = 10^{15}$ cm^{-2}. This effectively means that the neutral bulk region disappears and represents the point where both space charge regions meet. There seems to be no or little dependence of the y_{back} on annealing as well (see Fig. 6b). The fluence step shown is $\Phi_{eq} = 2 \cdot 10^{15}$ cm^{-2} and only after the last annealing step one can observe joining of the regions with opposite sign of the space charge; i.e. increase of y_{back}.

The drift velocity at the back of the detector increases almost linearly with applied bias voltage as shown in Fig. 6c. In all cases the bias voltage applied was lower than V_{fd}. As it can be seen $v_{back}/v_{sat} \approx 0.6$ after total fluence of $\Phi_{eq} = 1 \cdot 10^{16}$ cm^{-2} at 800 V, which corresponds to electric field > 1 V/μm.

4.3 Neutral bulk

The drift velocity in the so called "neutral bulk" is shown for all fluences and voltages investigated in Fig. 7. As can be seen the velocity increases with fluence and voltage. The velocity in the bulk reaches around one third of the saturated one. This translates to electric field strength of around > 0.3 V/μm. This is in agreement with observations made in Ref. [16]. Such a substantial electric field effectively means that at high fluences the whole detector is active.

5. Conclusions

A silicon micro-strip n-on-p type sensor was irradiated with neutrons to fluences up to $\Phi_{eq} = 1 \cdot 10^{16}$ cm^{-2}. Edge-TCT was used to extract the velocity profiles. The velocity profiles show the existence of two regions with opposite sign of the space charge and neutral bulk in
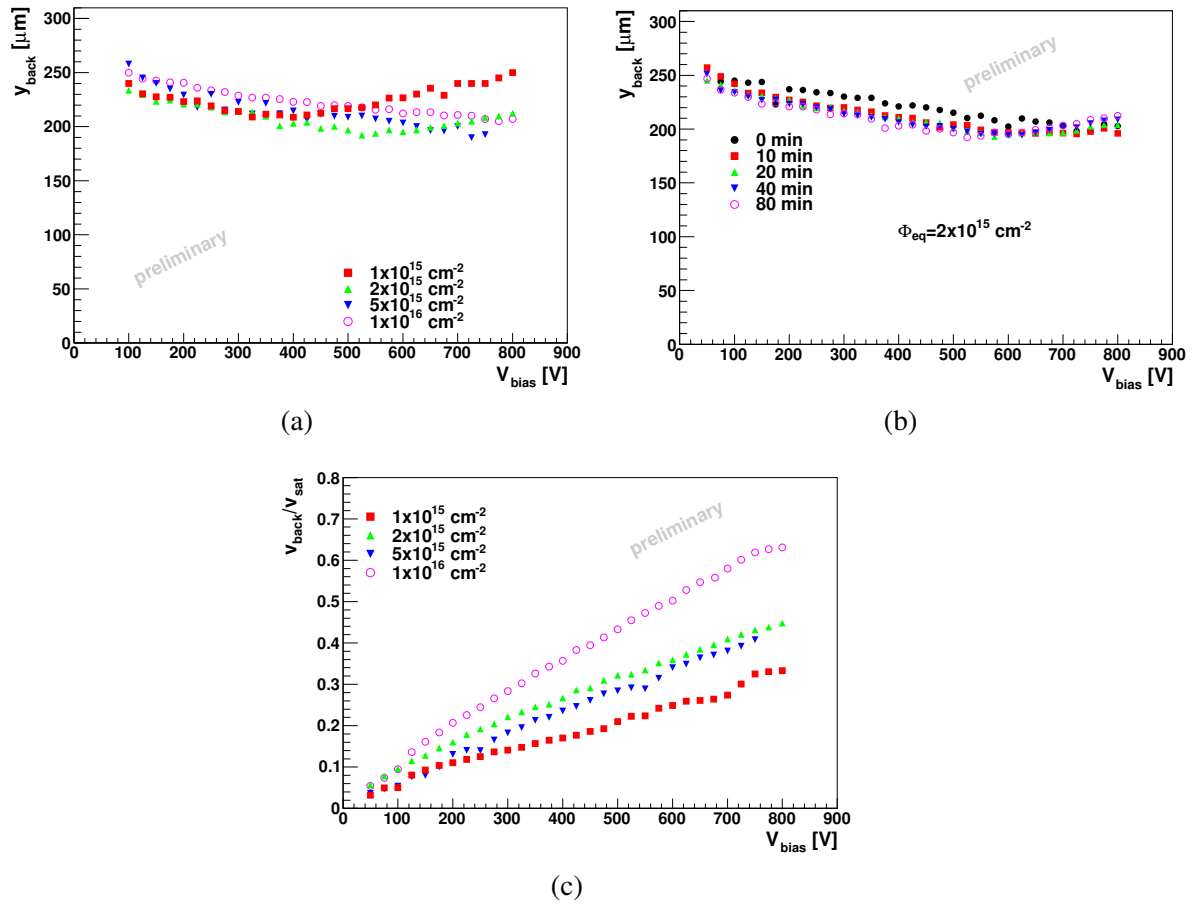
(a)

(b)

(c)

Figure 6: Dependence of y_{back} on voltage for: (a) different fluences after 80 min annealing (b) different annealing times for a detector at accumulated fluence of $2 \cdot 10^{15}$ cm^{-2}. (c) v_{back}/v_{sat} vs. voltage plot at different fluence steps.
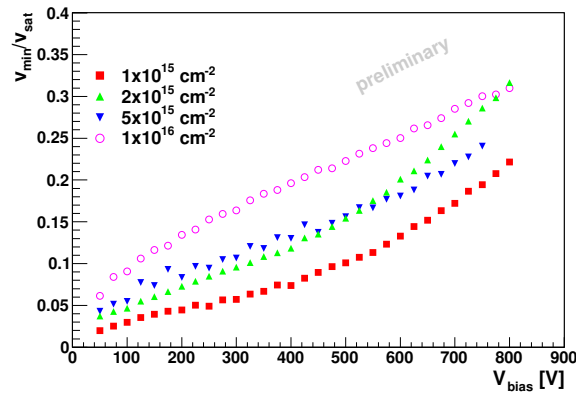

Figure 7: Dependence of drift velocity in the neutral bulk on voltage for different fluences.

between. The electric field was parametrized by a simple model assuming constant effective space charge at the junction and at the back electrode. The borders of the both regions, velocity in the

neutral bulk and at the back electrode were determined as a function of fluence and voltage. It was shown that the assumption of constant N_{eff} increasing linearly with fluence describes the velocity profiles adequately up to the fluences of $\Phi_{eq} < 2 \cdot 10^{15}$ cm^{-2}.

References

[1] F. Gianotti et al., hep-ph/0204087, 2002.

[2] G. Lindström et al., Nucl. Instr. and Meth. A 466 (2001) p. 308.

[3] C. Da Via, S.J. Watts, Nucl. Instr. and Meth. A 501 (2003) p. 138.

[4] G. Casse et al., Nucl. Instr. and Meth. A 624 (2010) p. 396.

[5] F. Hartman et al., Nucl. Instr. and Meth. A 617 (2010) p. 543.

[6] I. Mandić et al., Nucl. Instr. and Meth. A 603 (2009) p. 263.

[7] G. Casse et al., "Can we claim charge multiplication in heavily irradiated segmented detectors?", presented at 14th RD-50 Workshop, Freiburg, Germany, 2009.

[8] M. Petasecca et al., Nucl. Instr. and Meth. A 563 (2006) p. 192.

[9] V. Eremin et al., Nucl. Instr. and Meth. A 476 (2002) p. 556.

[10] V. Eremin et al., Nucl. Instr. and Meth. A 372 (1996) p. 388.

[11] G. Kramberger et al., Nucl. Instr. and Meth. A 481 (2002) p. 297.

[12] O. Krasel et al., IEEE Trans. NS 51(1) (2004) 3055.

[13] G. Kramberger et al., IEEE Trans. Nucl. Sci. Vol. 57(4), 2010, p. 2294.

[14] L. Snoj et al., Appl. Radiat. Isot. 70 (2012) p. 483.

[15] D. Žontar et al., Nucl. Instr. and Meth. A 426 (1999) p. 51.

[16] I. Mandic et al., Nucl. Instr. and Meth. A 533 (2004) p. 442.

[17] V. Eremin et al., Nucl. Instr. and Meth. A 360 (2004) p. 458.

[18] D. Menichelli et al., Nucl. Instr. and Meth. A 426 (1999) p. 135.

[19] V. Cindro et al., Nucl. Instr. and Meth. A 599 (2009) p. 60.